Materials Today Bio 28 (2024) 101200

Contents lists available at ScienceDirect

Materials Today Bio

journal homepage: www.journals.elsevier.com/materials-today-bio

Illuminating the fight against breast cancer: Preparation and visualized photothermal therapy of hyaluronic acid coated ZIF-8 loading with indocyanine green and cryptotanshinone for triple-negative breast cancer

Zhe Li [a,c,1], Liyan Sun [a,1], Jinshuai Lan [a,c,1], Ya Wu [a], Siqi Yang [a], Tong Zhang [a,c,*], Yue Ding [a,b,c,**]

[a] School of Pharmacy, Shanghai University of Traditional Chinese Medicine, Shanghai, 201203, China
[b] National Innovation Platform for Medical Industry-education Integration, Shanghai University of Traditional Chinese Medicine, Shanghai, 201203, China
[c] State Key Laboratory of Integration and Innovation of Classic Formula and Modern Chinese Medicine, Shanghai University of Traditional Chinese Medicine, Shanghai, 201203, China

ARTICLE INFO

Keywords:
Breast cancer
Visualized photothermal therapy
ZIF-8
Indocyanine green
Cryptotanshinone
Glycolysis

ABSTRACT

Triple-negative breast cancer (TNBC) is characterized by higher recurrence rate and mortality. Thermally-mediated ablation via photothermal therapy (PTT) demonstrates considerable promise for the eradication of breast cancer. Nonetheless, the efficacy of PTT is impeded by the thermal tolerance of tumor cells, which is attributed to the augmented expression of heat shock proteins (HSPs). These proteins, which function as ATP-dependent molecular chaperones, confer protection to cancer cells against the cytotoxic heat generated during PTT. Glycolysis is an important way for breast cancer cells to produce ATP, which can promote the occurrence and development of lung metastasis of breast cancer. Therefore, inhibiting glycolysis may diminish the expression of HSPs, curtail the growth of breast cancer, and prevent its metastasis. Glycolytic metabolism plays a pivotal role in the ATP biosynthesis within breast cancer cells, facilitating the progression and dissemination of pulmonary metastases. Consequently, targeting glycolysis presents a strategic approach to HSP expression, the proliferation of breast cancer, and impede its metastatic spread. Herein, we designed an indocyanine green (ICG) and cryptotanshinone (CTS) loaded hyaluronic acid (HA) coated Zeolitic Imidazolate Framework-8 (ZIF-8) drug delivery system. The drug delivery system had excellent photothermal properties, which could reach temperature sufficient for photothermal ablation of tumor cells. (ICG + CTS)@HA-ZIF-8 also showed pH-responsive drug release, enhancing the sustained release of ICG and CTS to extend their systemic circulation duration. Moreover, the HA modification of ZIF-8 served to augment its targeting capabilities both *in vitro* and *in vivo*, leveraging the enhanced permeation and retention (EPR) effect, as well as active tumor targeting via the CD44 receptor pathway, resulting in a higher drug concentration and a better therapeutic effect in tumor. (ICG + CTS)@HA-ZIF-8 could downregulate the expression of glycolysis-related protein pyruvate kinase-M2 (PKM2), thereby inhibiting the glycolysis process, further suppressing tumor cell energy metabolism, downregulating the expression of HSPs, overcoming tumor cell heat resistance, and improving PTT effect. It exhibited a notable suppressive impact on both the proliferation and migration of breast cancer cells, potentially offering innovative insights for the visualized PTT in breast cancer treatment.

1. Introduction

Breast cancer stands as a critical oncological challenge impacting women's health. According to International Agency for Research on Cancer, the global incidence of breast cancer in 2020 was recorded at roughly 2.26 million new cases, which constituted 24.5 % of all new cancer diagnoses among females worldwide in that year. The mortality of breast cancer ranks fifth in the world with fatalities reaching 680,000

* Corresponding author. School of Pharmacy, Shanghai University of Traditional Chinese Medicine, Shanghai, 201203, China
** Corresponding author. School of Pharmacy, Shanghai University of Traditional Chinese Medicine, Shanghai, 201203, China.
E-mail addresses: zhangtongshutcm@hotmail.com (T. Zhang), Dingyue-2001@hotmail.com (Y. Ding).
[1] These authors contributed equally to this work.

https://doi.org/10.1016/j.mtbio.2024.101200
Received 24 April 2024; Received in revised form 6 August 2024; Accepted 9 August 2024
Available online 10 August 2024

[1,2]. Microarray-based expression profiling revealed that breast cancer had five intrinsic subgroups, with triple-negative breast cancer (TNBC) accounting for 15–20 % of all invasive breast cancer subtypes. Distinguished by the lack of estrogen receptors (ER), progesterone receptors (PR), and human epidermal growth factor receptor 2 (HER-2) on the cancer cellular membranes, TNBC presents unique challenges for treatment. Due to its high metastasis, poor prognosis, lack of therapeutic targets, TNBC exhibits a higher recurrence rate and mortality [3]. For TNBC patients, systemic treatment may be a better treatment option compared to surgery [4]. TNBC is sensitive to chemotherapy, and the current chemotherapy standards are anthracylines and taxanes [4]. However, still, 30%–40 % of early TNBC patients experience metastasis and ultimately die from cancer, and chemotherapy has poor specificity and strong side effects. Radiotherapy inevitably causes damage to healthy tissues during treatment. The use of molecular targeted anti-tumor drugs also easily leads to drug resistance, which greatly restricts its clinical use [3,5]. Despite adherence to the tailored protocols of the Fudan University Shanghai Cancer Center for TNBC, the objective response rate (ORR) was merely 29.0 % [6], underscoring the urgent need for the development of treatment strategies for TNBC that are highly targeted, minimally toxic, non-invasive, and efficacious.

Photothermal therapy (PTT), an emerging modality in oncological treatments, is garnering interest as it is a relatively "mild" approach. PTT has shown great potential in ablating solid tumors and has been implemented in various cancer treatments, including breast cancer [7]. Tumor cells exhibit heightened thermal sensitivity compared to their normal counterparts. Heat can compromise the integrity of the tumor cell membrane, disrupt DNA replication, trigger immune responses, and alter the tumor microenvironment, leading to tumor cell necrosis and apoptosis, which is the premise for the application of PTT in cancer treatment [8]. Indocyanine green (ICG) is a water-soluble photosensitizer approved by the FDA for clinical use, and it is the only near-infrared (NIR) dye used for human vascular optical imaging. ICG has excellent photothermal conversion ability and near-infrared fluorescence imaging performance under 808 nm laser irradiation, making it widely used in PTT and fluorescence imaging research. However, free ICG has limitations such as aggregation tendency, poor photo stability, poor targeting ability and rapid *in vivo* excretion, which restricts its application in tumor PTT. Moreover, single PTT also has certain limitations: tumor cells treated with PTT will abnormally express various heat shock proteins (HSPs), such as HSP70 and HSP90, to resist thermal damage, resulting in insufficient apoptosis and poor tumor treatment efficacy. Consequently, it is essential to explore combined therapeutic approaches that can overcome tumor heat resistance and enhance the therapeutic efficacy of PTT. Previous research indicated that therapeutic agents such as RNA interference (RNAi) or specific inhibitors to inhibit the production of HSPs could be used for the treatment of tumor heat resistance. Dai et al. developed a NIR-II light-activated nanomedicine by co-encapsulating the HSP90 inhibitor gambogic acid and azoic compound, which effectively inhibited the action of HSP90 in cells during PTT and improved the thermal sensitivity of tumor cells. Wang et al. designed a nanoparticle with gold nanoshell to load HSP70 small interfering RNA (siRNA), which significantly suppressed the expression of HSP70 in cells by silencing the relevant genes, enhancing the PTT effect. However, these methods had many limitations. Firstly, siRNA or inhibitors could only target specific HSPs, lacking universality. Secondly, directly targeting HSPs themselves was a lagging process that weakened its inhibitory effect, lacking timeliness. We need to explore more effective methods to completely inhibit HSPs and achieve ideal PTT effects. Therefore, the combination of multiple drugs or treatment modes with ICG to construct a multi-mode synergistic PTT system is of great significance.

The energy required by cells is mainly supplied by the oxidation of glucose. Unlike normal cells, most tumor cells prefer glycolysis over oxidative phosphorylation for energy production, a preference that persists even in oxygen-rich conditions. This phenomenon, known as the Warburg effect, was first identified by Otto Warburg [9]. Breast cancer cells, similar to most tumor cells, primarily rely on glycolysis for the generation of adenosine triphosphate (ATP). It has been demonstrated in prior research that the disruption of breast cancer cell energy metabolism by targeting glycolytic enzymes can markedly curb breast cancer growth and metastasis [10–12]. HSPs are ATP-dependent chaperone proteins, whose synthesis, expression and function also depend on the level of ATP. Within the glucose metabolism pathway, pyruvate kinase-M2 (PKM2) in tumor cells catalyzes the transfer of a high-energy phosphate bond of phosphoenolpyruvate to adenosine diphosphate, generating ATP [13]. Therefore, silencing PKM2 can throttle the glycolytic pathway of breast cancer cells, weaken their energy metabolism, disrupting the ATP supply necessary for HSP production, and consequently reducing tumor cell heat resistance to PTT [14,15]. In summary, targeting glycolysis to deplete glucose in breast cancer cells can decrease their metabolic activity. This not only impedes tumor growth but also obstructs HSP production, thereby overcoming thermal resistance, hindering metastasis, and bolstering the effectiveness of PTT.

The latest research showed that cryptotanshinone (CTS), a bioactive compound isolated from the traditional Chinese medicine *Salvia miltiorrhiza* Bge., could downregulate the expression of the glycolysis-associated protein PKM2, thereby inhibiting the glycolysis process and subsequently suppressing tumor cell energy metabolism, exhibiting pronounced efficacy in hindering the proliferation, migration, and invasion of breast cancer cells [16]. Based on these, we hypothesised that the combination of ICG and CTS could inhibit the glycolysis process, thereby suppressing tumor cell energy metabolism, blocking the generation of HSPs, overcoming the heat resistance of tumor cells, not only curtailing the proliferation of breast cancer, but also inhibiting the metastasis of breast cancer, and amplifying the efficacy of PTT. However, the key issue is how to achieve efficient targeted delivery of ICG and CTS. The use of nanocarriers for co-delivery of drugs in anticancer combination therapy has great potential, as nanocarriers can ensure that the components of the drugs reach the target site as expected to maximize their synergistic anticancer effects.

Wang et al. constructed an ICG loaded Zeolitic Imidazolate Framework-8 (ICG@ZIF-8) therapeutic system using a "one-pot" approach. The fabricated ICG@ZIF-8 exhibited excellent photothermal effect and infrared fluorescence imaging function, extremely high ICG loading capacity, and outstanding photothermal stability [17]. ICG@ZIF-8 also had pH sensitivity, indicating its stability in neutral or alkaline conditions while rapidly decomposing in acidic environments owing to protonation, which suggested that ZIF-8 could be used as a nanocarrier for co-delivery of ICG and CTS in anticancer combination therapy. Nonetheless, the application of ZIF-8 in biomedicine is hindered by its inherent shortcomings, such as proneness to aggregation, suboptimal water dispersibility, and an absence of functional groups on the surface, limit its application in the field of biomedicine. Research has suggested that the utility of ZIF-8 in drug delivery systems may largely depend on enhancing its surface stability, augmenting its hydrophilicity, and improving its biocompatibility and specific surface functionality. Hyaluronic acid (HA) is a naturally existing, negatively charged, hydrophilic polysaccharide that possesses various desirable characteristics, including biocompatibility, biodegradability and non-immunogenicity, particularly exhibiting a high affinity for the cell surface CD44 receptor. Researchers have demonstrated that CD44 is overexpressed on the surfaces of most tumor cells, including 4T1 cells. Therefore, the encapsulation of ZIF-8 with HA can enhance its dispersibility, stability, and delivery efficiency [16].

Based on the research background and existing problems mentioned above, combined with the properties and pharmacological effects of CTS and photothermal agent ICG, we designed a HA coated ZIF-8 loading with ICG and CTS ((ICG + CTS)@HA-ZIF-8). (ICG + CTS)@HA-ZIF-8 not only solved the problems of ICG's photo stability, targeting ability and rapid *in vivo* excretion, but also improved the delivery of hydrophobic drug CTS. It enabled co-loading of hydrophilic and hydrophobic drugs,

secured efficient drug concentration at the tumor site via the enhanced permeation and retention (EPR) effect and CD44-mediated tumor active targeting, and realized maximum PTT effect. In view of the heat resistance faced by tumor PTT, this delivery system could downregulate the expression of glycolysis-related protein PKM2, thereby inhibiting the glycolysis process, further suppressing tumor cell energy metabolism, downregulating the expression of HSPs, overcoming tumor cell heat resistance, and improving PTT effect. It exhibited a potent suppressive impact on the proliferation, migration, and invasion of breast cancer cells, potentially offering novel insights for the visualized photothermal treatment of breast cancer.

2. Experimental section

2.1. Materials

Shanghai Energy Chemical Co., Ltd. (Shanghai, China) provided ICG, while 2-Methylimidazole (2-Mim) and $Zn(NO_3)_2•6H_2O$ and methanol were obtained from Sinopharm Chemical Reagent Co., Ltd. (Shanghai, China). CTS was procured from Shanghai Yuanye Biotechnology Co.,Ltd (Shanghai, China). Beyotime Biotechnology (Shanghai, China) supplied the CCK-8, Hoechst 33342, Annexin V-FITC/PI Apoptosis, Glucose Assay Kit and ATP Assay Kits. All antibodies used in the western blotting assay were acquired from Abcam.

4T1 cell line was obtained from the Cell Bank of Typical Culture Preservation Committee of the Chinese Academy of Sciences (Shanghai, China). 4T1 cells were preserved in 1640 medium, enriched with 10 % FBS and 1 % penicillin/streptomycin, cultured at 37 °C in an atmosphere containing 5 % CO_2.

2.2. Ethics statement

All experiments involving animals were conducted according to the ethical policies and procedures approved by the Animal Ethics Committee of Shanghai University of Traditional Chinese Medicine prior to commencement with the ethical approval number of PZSHUTCM2305300003. All procedures involving animals were conducted in strict adherence to the guidelines for the care and use of laboratory animals. The study concluded with the euthanasia of the animals via cervical dislocation under isoflurane anesthesia.

2.3. Preparation and characterization of (ICG + CTS)@HA-ZIF-8

The ICG@ZIF-8 was synthesized using the "one-pot method" as reported in the previous research with lightly change [18]: $Zn(NO_3)_2•6H_2O$ (150 mg) and ICG (42 mg) were solubilized in 7.3 mL of methanol. 2-Mim (330 mg) was dissolved in 7.15 mL of methanol. Then, the 2-Mim solution was then gradually introduced into the mixed solution of $Zn(NO_3)_2•6H_2O$ and ICG under vigorous stirring (500 rpm) at ambient temperature for 5 min. The resultant ICG@ZIF-8 was isolated via centrifugation at 12000 rpm for 5 min, followed by a dual methanol wash until the supernatant appeared transparent. Subsequently, 50 mg of synthesized ICG@ZIF-8 was incorporated into a CTS solution (10 mg/mL) and stirred vigorously at 500 rpm for 24 h at room temperature. (ICG + CTS)@ZIF-8 was then collected through centrifugation at 12000 rpm for 5 min and washed twice with methanol. Finally, 50 mg of the prepared (ICG + CTS)@ZIF-8 was dispersed in 5 mL of 10 % HA solution under strong stirring (500 rpm) at room temperature for 24 h, and further purified by centrifugation at 12000 rpm for 5 min to get (ICG + CTS)@HA-ZIF-8. The preparation of CTS@ZIF-8, ICG@HA-ZIF-8 and CTS@HA-ZIF-8 referred to the above methods with/without ICG or CTS addition during the preparation process. The drug loading process was conducted based on the results of ICG and CTS used in combination (Fig. S1 and **Table S1**). The prepared (ICG + CTS)@ZIF-8 and (ICG + CTS)@HA-ZIF-8 were appropriately dispersed and diluted for the measurement of particle size and Zeta potential using the Malvern Zetasizer ZEN3600 Nano ZS system (Malvern Instruments, Malvern, UK). Transmission electron microscopy (TEM) (SEMC, New York, USA) was employed to observe the morphology of the formulations. FTIR spectrum was also used to confirm HA coating on the surface of (ICG + CTS)@ZIF-8. Concentrations of ICG and CTS in the samples was determined by UV–Vis spectrophotometry and highformance liquid chromatography (HPLC), respectively (Fig. S2). Calculation of the drug loading efficiency for ICG and CTS in these preparations was performed. To evaluate the photothermal performance of the formulations, PBS, ICG, ICG@HA-ZIF-8, CTS@HA-ZIF-8, (ICG + CTS)@ZIF-8 and (ICG + CTS)@HA-ZIF-8 (concentration of ICG = 15 μg/mL) were subjected to an 808 nm laser at a power density of 1.0 W/cm^2. Infrared thermal imaging was utilized to record temperature fluctuations. To evaluate the photothermal stability of ICG and (ICG + CTS)@HA-ZIF-8, the formulations were exposed to the 808 nm laser at 1.0 W/cm^2 for 2 min, followed by a cooling period of 4 min. This process was repeated for four times. Infrared images and temperature profiles were documented during these intervals. Further, the photothermal conversion efficacy for ICG and (ICG + CTS)@HA-ZIF-8 was investigated by laser irradiation at the same wavelength and power for 5 min to attain peak temperature, after which the laser was deactivated. During this period, photographs were taken with an infrared camera and temperature change curves were plotted. From these data, the photothermal conversion efficiency (η) was determined.

2.4. pH-sensitive drug release study

To assess the release of ICG and CTS from ICG + CTS, (ICG + CTS)@ZIF-8, and (ICG + CTS)@HA-ZIF-8, the formulations were placed in 20 mL of PBS at pH levels of 5.5 and 7.4, both solutions supplemented with 0.5 % sodium dodecyl sulfate, shaking with the speed of 100 rpm at 37 °C for 24 h. 1 mL aliquots were withdrawn at 0, 5, 15, 30, 60, 120, 240, 640, 720, and 1440 min, respectively, and an equivalent volume of release medium at the same temperature was promptly replenished. After filtering through a 0.45 μm millipore filter, and the resulting filtrates were analyzed for the concentrations of ICG and CTS using UV–visible spectrophotometry or HPLC.

2.5. In vitro cellular uptake

Before conducting *in vitro* cell studies, we first assessed the biosafety of ZIF-8 and HA-ZIF-8 in 4T1 cells. To ascertain the impact of laser exposure and HA coating on the uptake of the formulation, 4T1 cells were employed to analyze the uptake ability of various formulations using flow cytometry and confocal laser scanning microscopy (CLSM). In the flow cytometric analysis, 4T1 cells were seeded at a density of 2 × 10^5 cells/mL in a 6-well plate and cultured overnight. Subsequently, the cells were treated with 1 mL of culture medium containing the respective formulation (normalizing the concentration of ICG in each formulation to 2.44 μM). The cells were incubated at 37 °C for 2, 4, or 6 h, after which they were harvested and the ICG fluorescence was measured via flow cytometry to evaluate the uptake efficiency. For CLSM study, 4T1 cells were seeded at a density of 1 × 10^5 cells/mL in a glass-bottom Petri dish and cultured overnight. Then, 1 mL of culture medium containing the formulation (normalizing the concentration of ICG in each formulation to 10 μM) was added and incubated at 37 °C for optimized time. Post incubation, the culture medium was removed, cells were rinsed thrice with PBS, fixed with 4 % paraformaldehyde for 10 min, and stained for 20 min at room temperature with Hoechst 33342. Finally, the cells were imaged using CLSM to visualize the uptake of formulations.

2.6. In vitro cytotoxicity study

In a 96-well plate, 4T1 cells were seeded at a density of 8 × 10^3 cells/mL and cultured overnight. The groups were as follows: ICG, ICG(+L), CTS, ICG + CTS(+L), ICG@HA-ZIF-8(+L), CTS@HA-ZIF-8, (ICG + CTS)

@ZIF-8(+L), (ICG + CTS)@HA-ZIF-8 and (ICG + CTS)@HA-ZIF-8(+L). The cells were incubated with various formulations. After incubation for optimized time mentioned above, the groups with "(+L)" underwent irradiation using an 808 nm laser at 1.0 W/cm^2 for optimized time mentioned above, followed by further incubation for 24 h. Subsequently, CCK-8 solution was then dispensed into each well, and the cells were allowed to incubate in absence of light for 1.25 h. Absorbance at 450 nm was determined using a microplate reader (Biotek, USA). The growth inhibition rate of the formulations on 4T1 cells was calculated.

2.7. Cell apoptosis study

4T1 cells were seeded in a 6-well plate at a density of 5 × 10^5 cells/mL and cultured overnight. Different formulations were added and incubated (drug concentration calculated as 2 μM based on ICG), and after incubation for optimized time mentioned above, the groups with "(+L)" were then exposed to an 808 nm laser at 1.0 W/cm^2 for optimized time mentioned above, followed by incubation for an additional 24 h. The cells were digested with trypsin without EDTA and then collected by centrifugation. The cells were subsequently stained with Annexin V-FITC/PI for apoptosis analysis, which was conducted through flow cytometry.

2.8. Inhibition of tumor cell migration

An assessment of the various formulations' effects on 4T1 cell migration was conducted using a wound healing experiment. 4T1 cells were seeded in a 6-well plate at a density of 5 × 10^5 cells/mL and cultured overnight. When the density of 4T1 cells reached 90 %, a straight scratch line was drawn. The scratch area was gently rinsed multiple times with PBS to remove detached cells and then evaluated and imaged using an optical microscope. The culture medium was replaced with different formulations (drug concentration calculated as 1.5 μM based on ICG) and incubated for optimized time mentioned above. The groups with "(+L)" were exposed to an 808 nm laser at 1.0 W/cm^2 for optimized time mentioned above, followed by a 24 h post-irradiation incubation. Microscopic observations of the wound healing were made, and corresponding images were captured. The Image J software facilitated the analysis of the images, quantifying the wound area reduction, which was then used to calculate the percentage of wound healing.

2.9. Measurement of intracellular glucose uptake and ATP level

4T1 cells were seeded in a 6-well plate at a density of 5 × 10^5 cells/mL and cultured overnight. Varying formulations were added (concentration of CTS = 7 μM) and incubated for optimized time mentioned above, the groups with "(+L)" underwent 808 nm laser irradiation at 1.0 W/cm^2 for optimized time mentioned above, continued to incubate for an additional 24 h. The culture medium was then removed. The cells were trypsinized, collected by centrifugation, lysed, and subsequently subjected to centrifugation to obtain the supernatant, which was then utilized for the quantification of intracellular glucose uptake and ATP levels using the Glucose Assay Kit and ATP Assay Kit.

2.10. In vitro detection of PKM2 and HSPs by western blot

4T1 cells were seeded in a 6-well plate at a density of 5 × 10^5 cells/mL and cultured overnight. Various formulations were added and incubated (concentration of ICG = 2 μM), and incubated for optimized time mentioned above. The groups with "(+L)" received 808 nm laser exposure at 1.0 W/cm^2 for optimized time mentioned above. After irradiation, the culture medium was removed, and the cells were collected after digestion with trypsin. The expression of the glycolytic key regulatory enzyme PKM2 and HSP70/90 in the cells was detected using WB.

2.11. In vivo tumor targeting and NIR-II fluorescence imaging

In vivo distribution experiments were conducted using mice bearing orthotopic 4T1 tumors to confirm the time of laser *in vivo* after drug administration and evaluate the tumor targeting of the formulations. Once the tumors reached approximately 150 mm^3, mice were randomly allocated into ICG, ICG@ZIF-8 and ICG@HA-ZIF-8 groups (n = 3). Post-intravenous administration of the respective formulations via the tail vein, the mice were anesthetized with 1.5 % isoflurane, and the fluorescence distribution and intensity of ICG in the mice was recorded at 0, 0.5, 1, 2, 4, 6, 8, 24 h post injection using the IVIS Lumina *in vivo* imaging system. At 24 h post-injection, the mice were euthanized, sacrificed, and their vital organs, including the heart, liver, spleen, lungs, kidneys, and the tumor tissues, were excised. After rinsing these specimens with saline, the biodistribution of the formulations in both the primary organs and tumor tissues was documented using the IVIS Lumina *in vivo* imaging system.

Following the establishment of the peak accumulation timeframe of the formulation within the body, the *in vivo* photothermal properties of the formulations were assessed using mice bearing orthotopic 4T1 tumors. When the tumor reached around 150 mm^3, the mice were segregated randomly into saline, ICG, ICG@ZIF-8 and ICG@HA-ZIF-8 groups (n = 3). The above formulations were administered via tail vein injection. After administration for determined time, the tumor sites of mice were exposed to an 808 nm laser at 1.0 W/cm^2. An infrared camera was used to monitor the temperature variations at the tumor sites.

2.12. In vivo anticancer efficacy of (ICG + CTS)@HA-ZIF-8

In vivo anti-tumor growth and metastasis pharmacological studies were conducted using mice bearing orthotopic 4T1 tumors. Once the tumor reached about 50 mm^3, mice were randomly stratified into various groups: saline, DOX, ICG + CTS(+L), CTS@HA-ZIF-8, ICG@ZIF-8(+L), (ICG + CTS)@ZIF-8(+L), (ICG + CTS)@HA-ZIF-8 and (ICG + CTS)@HA-ZIF-8(+L) groups (n = 5, dosage of ICG = 1.2 mg/kg, dosage of DOX = 2 mg/kg). The mice were administered with the formulations once every two days through tail vein injections over 18 days. The groups with "(+L)" received 808 nm laser irradiation at 1.0 W/cm^2 for determined time 1 h after injection. Body weight and tumor size of the mice were monitored every other day throughout the treatment period. After treatment, the mice were euthanized, sacrificed, and their primary organs and tumors were harvested. The tumors were cleansed, imaged, weighed, and subjected to Hematoxylin&Eosin (HE) staining. Ki67 and TUNEL of tumor tissues were also determined with immunohistochemical assay. At the same time, the tumor tissues were used for WB analysis and immunofluorescence staining to examine the expression of PKM2 and HSPs. The lung tissues of the mice were collected, rinsed with saline, stained with picric acid, photographed under a microscope, and the metastatic nodules were counted. The lung tissues were also immersed in 4 % polyformaldehyde solution and stained with HE to further analyze the metastatic foci in the lung tissues. The biological safety of the formulation was examined by the mouse weight change and HE staining of the main organs.

Referring to the above pharmacological experiments for grouping and administration (n = 5), the behavior status, tumor volumes, and death of the mice were observed within a month. Survival rates were depicted using Kaplan-Meier curves, and Median Survival Times (MeST) were determined to evaluate the comparative efficacy of each formulation on mice with orthotopic 4T1 tumors. According to the requirements related to experimental animal welfare, when the mouse weight decreased by more than 15 %, severe paralysis, tumor volume>1500 mm^3 or not eating for more than 48 h occurred, it was judged as animal death and euthanasia was implemented.

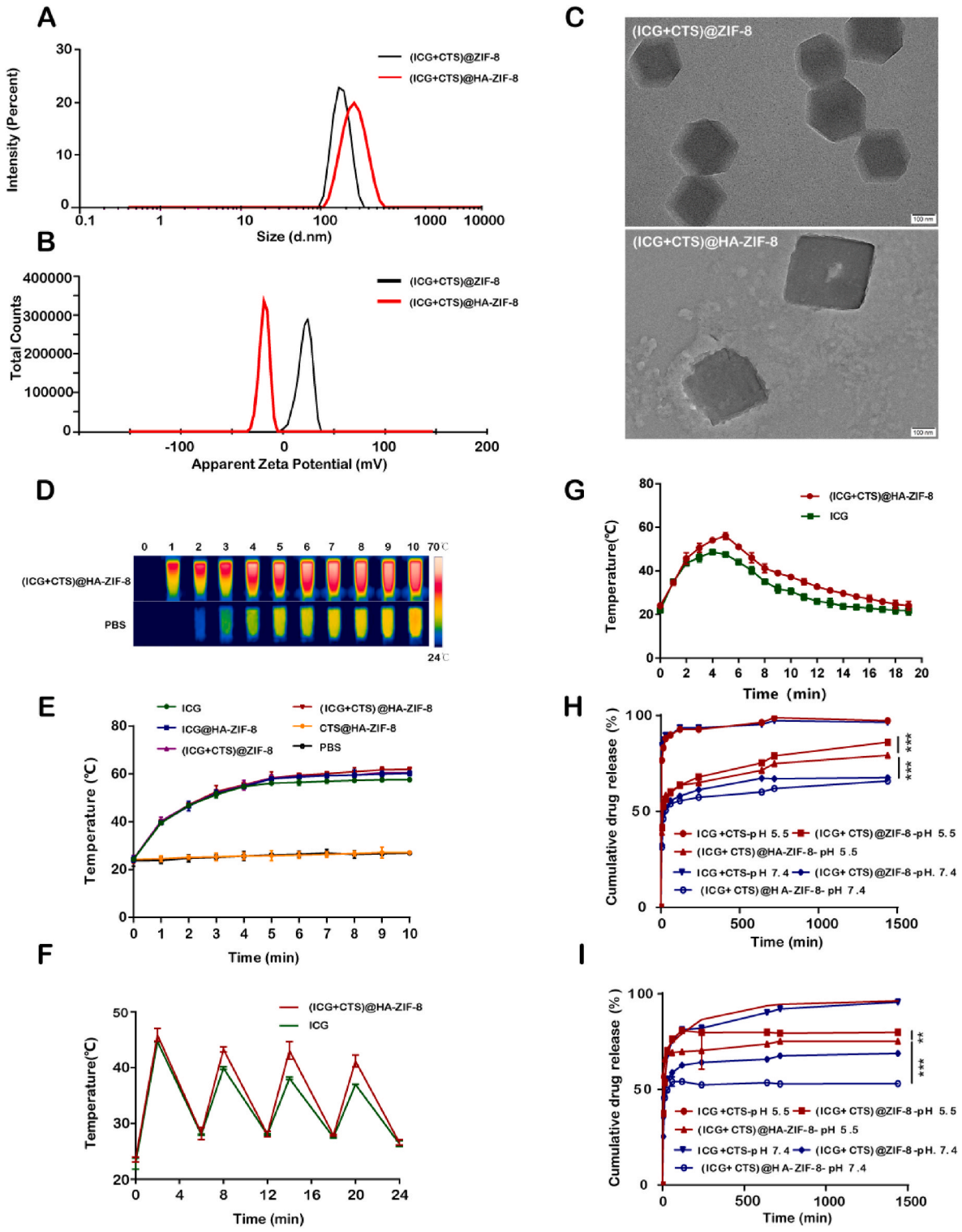

Fig. 1. Characterization and *in vitro* drug release study: A) Hydrodynamic particle size of (ICG + CTS)@ZIF-8 and (ICG + CTS)@HA-ZIF-8. B) Zeta potential of (ICG + CTS)@ZIF-8 and (ICG + CTS)@HA-ZIF-8. C) TEM images of (ICG + CTS)@ZIF-8 and (ICG + CTS)@HA-ZIF-8. Scale bar = 100 nm. D) Infrared thermal images of PBS and (ICG + CTS)@HA-ZIF-8 (concentration of ICG = 15 μg/mL) upon laser irradiation by 808 nm laser (1.0 W/cm^2) for 10 min. E) Time-dependent temperature elevation curves of PBS, ICG, ICG@HA-ZIF-8, CTS@HA-ZIF-8, (ICG + CTS)@ZIF-8 and (ICG + CTS)@HA-ZIF-8 (concentration of ICG = 15 μg/mL) upon laser irradiation by 808 nm laser (1.0 W/cm^2) for 10 min. F) Temperature variation of ICG and (ICG + CTS)@HA-ZIF-8 dispersion during cyclic laser exposure. (concentration of ICG = 15 μg/mL) G) Temperature variation of ICG and (ICG + CTS)@HA-ZIF-8 dispersion during laser irradiation by 808 nm laser (1.0 W/cm^2) for 5 min and after withdrawing laser. (concentration of ICG = 15 μg/mL) H) *In vitro* cumulative release profiles of ICG from free ICG + CTS, (ICG + CTS)@ZIF-8, and (ICG + CTS)@HA-ZIF-8 in release medium of 20 mL PBS with pH = 5.5 or PBS with pH = 7.4. I) *In vitro* cumulative release profiles of CTS from free ICG + CTS, (ICG + CTS)@ZIF-8, and (ICG + CTS)@HA-ZIF-8 in release medium of 20 mL PBS with pH = 5.5 or PBS with pH = 7.4. (*: $P < 0.05$, **: $P < 0.01$, ***: $P < 0.001$, n = 3).

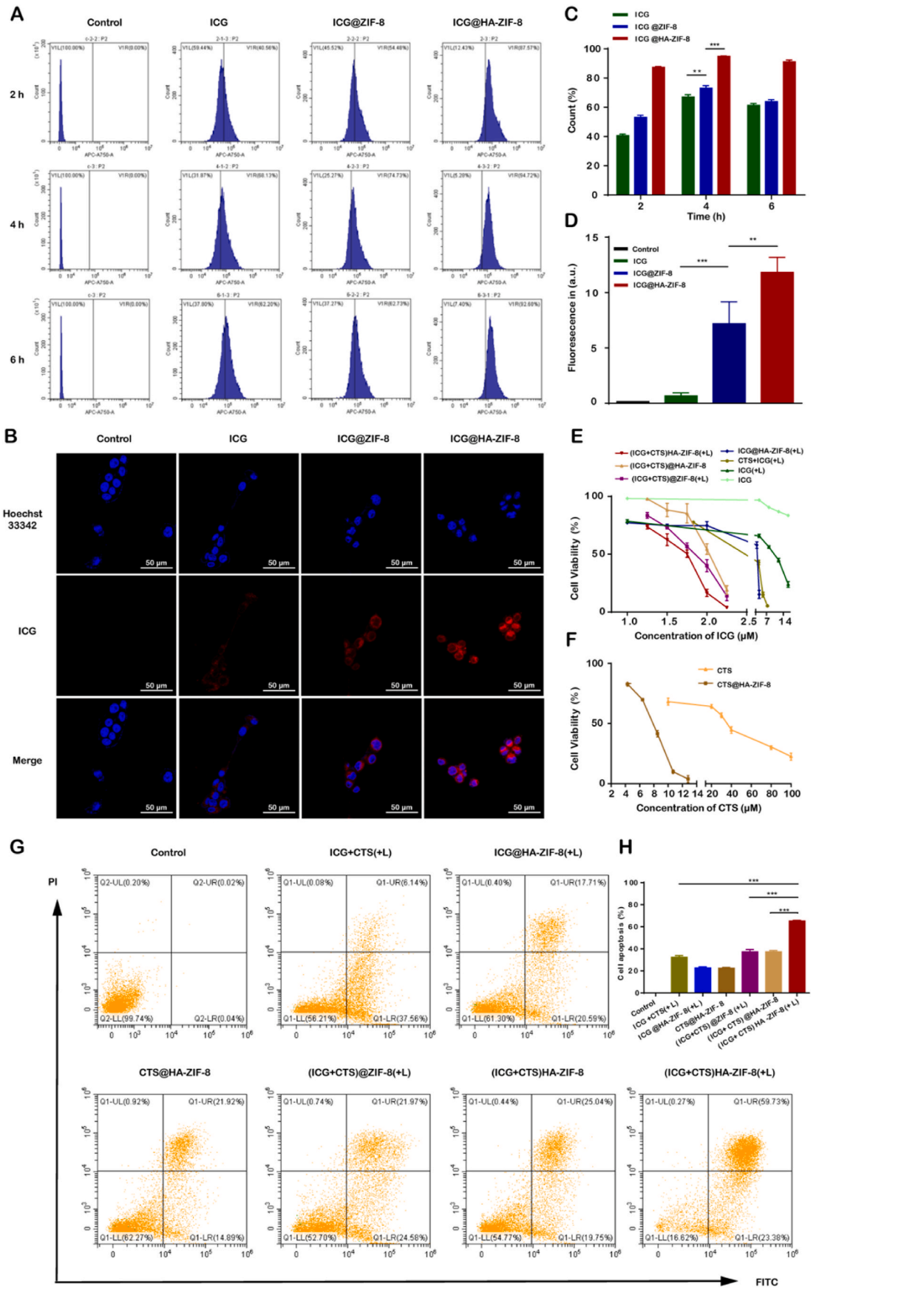

(caption on next page)

Fig. 2. *In vitro* cell uptake, cytotoxicity and cell apoptosis studies of different formulations in 4T1 cells: A) Cell uptake of ICG, ICG@ZIF-8 and ICG@HA-ZIF-8 by 4T1 cells with flow cytometry at 2, 4 or 6 h. B) Cell uptake of ICG, ICG@ZIF-8 and ICG@HA-ZIF-8 by 4T1 cells with CLSM at 4 h. C) The statistical quantification of detecting cell uptake of ICG, ICG@ZIF-8 and ICG@HA-ZIF-8 by 4T1 cell with flow cytometry. D) The statistical semi-quantification of detecting cell uptake of ICG, ICG@ZIF-8 and ICG@HA-ZIF-8 by 4T1 cell with CLSM. E) Cell viability of 4T1 cells after incubation with different formulations containing ICG at various concentrations with or without laser irradiation (808 nm, 1.0 W/cm^2, 5 min). F) Cell viability of 4T1 cells after incubation with formulations only containing CTS at various concentrations. G) The effect of different formulations on inducing 4T1 cell apoptosis. H) The statistical quantification of detecting cell apoptosis cell of different formulations on 4T1 cells. (*: $P < 0.05$, **: $P < 0.01$, ***: $P < 0.001$, n = 3).

2.13. Statistical analysis

The data are presented as mean ± SD. Differences among groups were performed with one-way ANOVA. $P < 0.05$ was considered statistically significant.

3. Results and discussion

3.1. Characterization of (ICG + CTS)@HA-ZIF-8

The particle size and Zeta potential of various formulations were quantified using a Malvern Zetasizer. The results were shown in Fig. 1A and B. The particle size of (ICG + CTS)@ZIF-8 was 192.5 ± 6.9 nm, with a PDI of 0.075 and a Zeta potential of 20.9 ± 6.67 mV. After HA coating, the particle size of (ICG + CTS)@HA-ZIF-8 was observed to enlarge to 224.4 ± 5.8 nm, with a PDI of 0.181 and the Zeta potential shifted to −19.6 ± 5.54 mV. These changes, including the increase in particle size and the shift from a positive to a negative charge, underscored the impact of the HA layer on the physical characteristics of (ICG + CTS)@ZIF-8. TEM was employed to examine the morphology of the nanoparticles. As shown in Fig. 1C, compared to (ICG + CTS)@ZIF-8, (ICG + CTS)@HA-ZIF-8 showed an increase in particle size and a rough surface, visually confirming the successful coating of HA. These results were consistent with previous literature [19]. As shown in Fig. S3, (ICG + CTS)@HA-ZIF-8 exhibited characteristic absorptions of HA at 2137.68 cm^{-1}, which further confirmed HA coating on the surface of (ICG + CTS)@ZIF-8. The drug loading of ICG and CTS in (ICG + CTS)@HA-ZIF-8 was 5.71 % and 3.58 %, respectively. Before further study, we Before further research, we examined the stability of the formulation in PBS. The results in Fig. S4 showed that (ICG + CTS)@ZIF-8 and (ICG + CTS)@HA-ZIF-8 were both stable within 7 days.

ICG, as a photothermal therapy agent, relies on the generation of heat under laser irradiation to achieve tumor ablation. The results showed that after 5 min of light exposure, the temperatures of ICG, (ICG + CTS)@ZIF-8 and (ICG + CTS)@HA-ZIF-8 were 56.1, 58.2, and 58.3 °C, respectively. In stark contrast, the PBS control group exhibited a minimal temperature increase to 26.1 °C (Fig. 1D and E). These observations affirm the potent photothermal capabilities of the ICG-containing formulations, efficiently converting light energy into heat within a short time, and surpassing the threshold temperature (>42 °C) necessary for the photothermal eradication of tumor cells [20]. One of the disadvantages of ICG is its poor stability. Improving the stability of ICG is crucial for enhancing its therapeutic efficacy [21]. Therefore, we compared the photothermal stability of ICG and (ICG + CTS)@HA-ZIF-8. As shown in Fig. 1F, (ICG + CTS)@HA-ZIF-8 maintained a high heat production effect after 4 circles of an 808 nm NIR light irradiation,at 1.0 W/cm^2, while pure ICG, although demonstrating good photothermal conversion ability during the first round of irradiation, quickly lost its near-infrared light absorption ability due to photobleaching effect after subsequent rounds of near-infrared light irradiation, resulting in a decrease in temperature from 44.7 °C to 37 °C. These findings suggested that encapsulating ICG into HA-ZIF-8 provided protection for ICG against photobleaching effect. The photothermal conversion effect is a prerequisite for the photothermal therapeutic effect of ICG. Therefore, we also investigated the *in vitro* photothermal conversion effect of (ICG + CTS)@HA-ZIF-8. The results, as shown in Fig. 1G, revealed that both free ICG and (ICG + CTS)@HA-ZIF-8 exhibited almost the same increase in temperature, with conversion efficiency η = 30.34 % for ICG and η = 37.75 %, or (ICG + CTS)@HA-ZIF-8, confirming that HA-ZIF-8 had no influence on the photothermal conversion efficiency of ICG.

3.2. pH-sensitive drug release in vitro

ZIF-8 is a metal framework material self-assembled by the coordination of Zn^{2+} and 2-Mim. The structure of ZIF-8 demonstrates stability within physiological pH yet disassembles in acidic conditions. Drug release profiles of the free ICG + CTS, (ICG + CTS)@ZIF-8, and (ICG + CTS)@HA-ZIF-8 examined within PBS at pH values of 5.5 and 7.4 to simulate the acidic environment of tumors and the normal physiological environment, respectively [17]. As shown in Fig. 1H and I, ICG and CTS released from (ICG + CTS)@ZIF-8 and (ICG + CTS)@HA-ZIF-8 slowly under pH = 7.4 condition. At 24 h, the release rates of ICG and CTS in (ICG + CTS)@ZIF-8 were only 67.63 % and 68.91 %, respectively. In (ICG + CTS)@HA-ZIF-8, the release rates of ICG and CTS were only 65.86 % and 53.07 %, respectively. In contrast, the release rates of ICG and CTS in free ICG + CTS reached 96.42 % and 95.74 %, respectively, denoting a significantly reduced drug seepage under physiological conditions for the encapsulated drugs. Under pH = 5.5 condition, the drug release rates were faster. At 24 h, the release rates of ICG and CTS in (ICG + CTS)@ZIF-8 reached 86.13 % and 79.87 %, respectively. In (ICG + CTS)@HA-ZIF-8, the release rates of ICG and CTS reached 79.32 % and 75.24 %, respectively. It was noteworthy that across both pH conditions, (ICG + CTS)@HA-ZIF-8 consistently exhibited a slower drug release in comparison to (ICG + CTS)@ZIF-8. This suggested that the HA coating on ZIF-8 serveed as a barrier, mitigating the release of ICG and CTS, which could be advantageous in prolonging the systemic circulation duration of the therapeutic agents [15].

3.3. In vitro cellular uptake

As shown in Fig. S5, ZIF-8 and HA-ZIF-8 were both safe under the concentration of 60 μg/mL. We conducted our subsequent experiments within this safe concentration range. HA component possesses a notable affinity for CD44 receptors, which are overexpressed on 4T1 cancer cells, suggesting that HA-modified ZIF-8 could potentially improve the targeting efficiency of the ZIF-8 delivery system. The uptake ability of 4T1 cells for each formulation was analyzed by flow cytometry and CLSM to investigate the influence of incubation time and HA coating on the uptake of formulations by 4T1 cells. The quantitative data from flow cytometry was shown in Fig. 2A and C, the fluorescence intensity of ICG peaked at 4 h for all formulations. Compared with ICG and ICG@ZIF-8, at 2, 4, and 6 h, 4T1 cells took up more ICG@HA-ZIF-8. At 4 h, the uptake of ICG@HA-ZIF-8 by 4T1 cells was significantly higher than that of ICG and ICG@ZIF-8 ($P < 0.05$), with uptake amounts 1.41 times and 1.30 times of ICG and ICG@ZIF-8, respectively. The possible reason was that HA could act as a targeting ligand, bind to CD44 receptors overexpressed on the surface of 4T1 cells, thus effectively promoting cell uptake. The qualitative analysis results of CLSM were shown in Fig. 2B and D, free ICG exhibited weaker red fluorescence compared to ICG@ZIF-8 and ICG@HA-ZIF-8, indicating that free ICG entered cells through passive diffusion, while nanoparticles enter cells through endocytosis, suggesting that endocytosis was more easily taken up by cells than passive diffusion, and HA coating formulation (ICG@HA-ZIF-8) was taken up more by 4T1 cells due to active targeting effect. Therefore, HA-ZIF-8 could deliver drugs into cells more effectively, providing a basis for a good therapeutic effect. As a result, in the

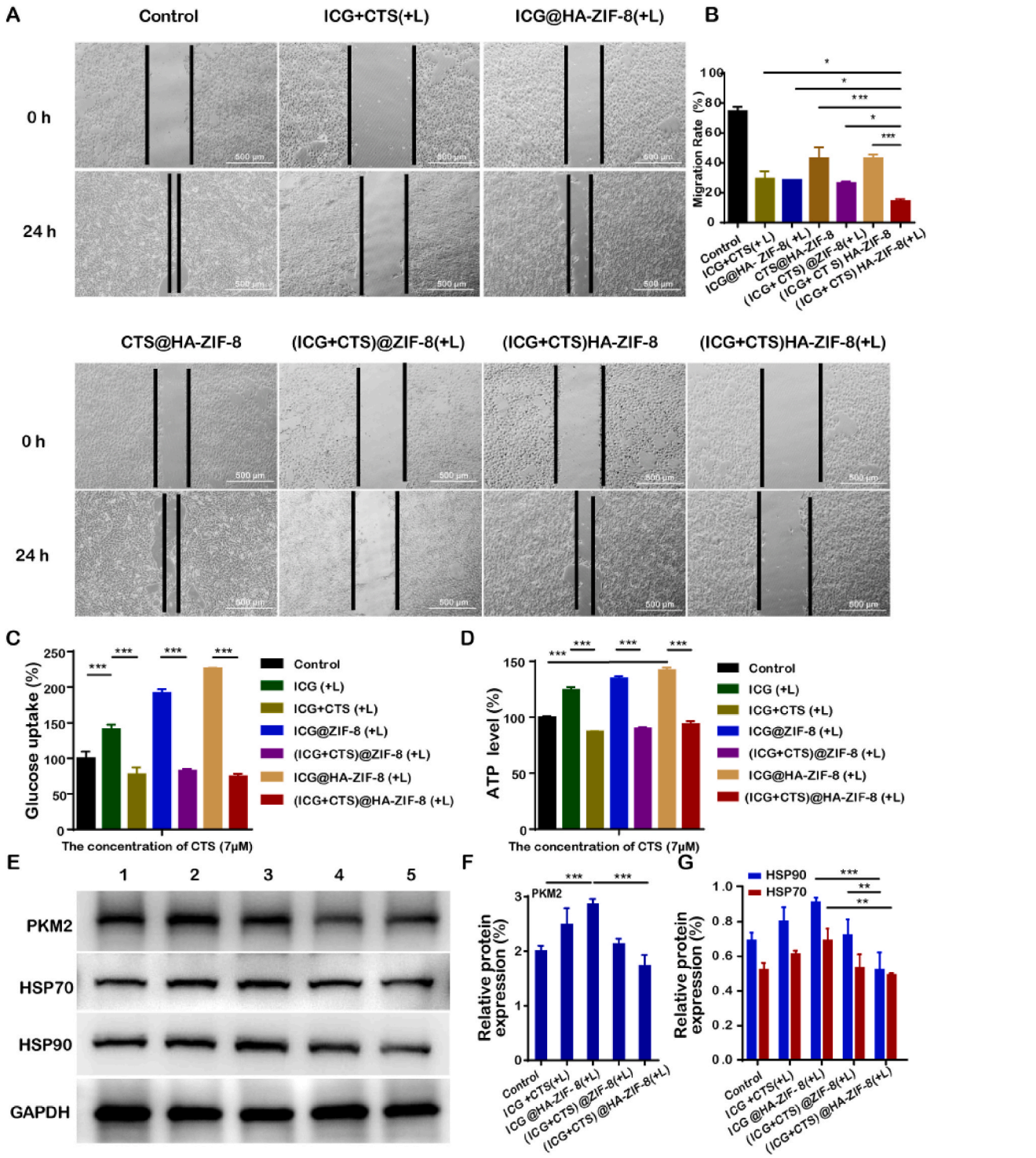

Fig. 3. *In vitro* anti-metastasis, intracellular ATP expression, quantitative glucose uptake, detection of PKM2 and HSPs expressions by WB of different formulations in 4T1 cells: A) The representative images of scratch wound-healing assays on 4T1 cell after treatment with different formulations. B) The statistical semi-quantification of scratch wound-healing assays on 4T1 cell after treatment with different formulations. C) Quantitative glucose uptake of 4T1 cells treated with ICG(+L), ICG + CTS (+L), ICG@ZIF-8(+L), (ICG + CTS)@ZIF-8(+L), ICG@HA-ZIF-8(+L) and (ICG + CTS)@HA-ZIF-8(+L) (concentration of CTS = 7 μM). D) The intracellular ATP expression of 4T1 cells treated with ICG(+L), ICG + CTS(+L), ICG@ZIF-8(+L), (ICG + CTS)@ZIF-8(+L), ICG@HA-ZIF-8(+L) and (ICG + CTS)@HA-ZIF-8(+L) (concentration of CTS = 7 μM). E) WB detection of PKM2 and HSP70/90 expressions in 4T1 cells after various treatments (1:Control; 2:ICG + CTS(+L); 3:ICG@HA-ZIF-8(+L); 4:(ICG + CTS)@ZIF-8(+L); 5:(ICG + CTS)@HA-ZIF-8(+L). F) The statistical semi-quantification of detecting PKM2 expression in 4T1 cells after various treatments. G) The statistical semi-quantification of detecting HSP70/90 expressions in 4T1 cells after various treatments. (*: $P < 0.05$, **: $P < 0.01$, ***: $P < 0.001$, n = 3).

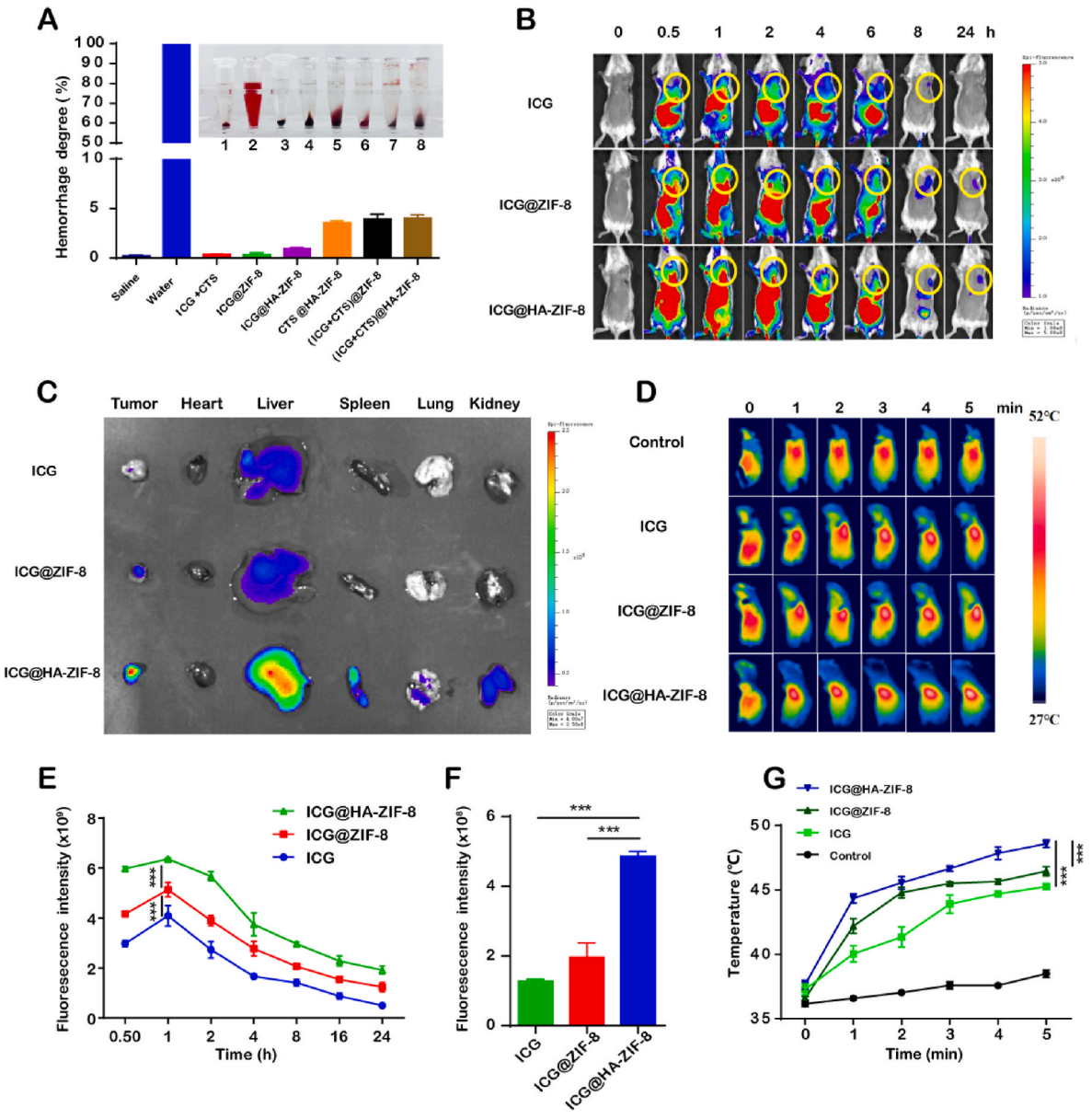

Fig. 4. *In vivo* hemolytic activity of the formulations, tumor targeting and NIR-II fluorescence imaging: A) *In vitro* hemolysis results of different formulations. (1: saline; 2:water; 3:ICG + CTS; 4:ICG@ZIF-8; 5:ICG@HA-ZIF-8; 6:CTS@HA-ZIF-8; 7:(ICG + CTS)@ZIF-8; 8:(ICG + CTS)@HA-ZIF-8) B) *In vivo* fluorescence imaging of mice bearing orthotopic 4T1 tumors injected intravenously with free ICG, ICG@ZIF-8 or ICG@HA-ZIF-8 at different time points. The yellow circles indicated the tumor sites. C) *Ex vivo* fluorescence imaging of excised tumors and organs at 24 h post-injection. D) Infrared thermal images of mice bearing orthotopic 4T1 tumors at 1 h post-intravenous injection of saline, free ICG, ICG@ZIF-8 or ICG@HA-ZIF-8 with laser irradiation (1.0 W/cm^2, 808 nm, 5 min). E) The fluorescence quantitation of tumors in mice bearing orthotopic 4T1 tumors at different time points. F) The fluorescence quantitation of excised tumors in mice bearing orthotopic 4T1 tumors at different time points. G) The temperature change curves of mice bearing orthotopic 4T1 tumors at 1 h post-intravenous injection of saline, free ICG, ICG@ZIF-8 or ICG@HA-ZIF-8 with laser irradiation (1.0 W/cm^2, 808 nm, 5 min). (*: $P < 0.05$, **: $P < 0.01$, ***: $P < 0.001$, n = 3). (For interpretation of the references to colour in this figure legend, the reader is referred to the Web version of this article.)

subsequent cell experiments, in order to maximize the enrichment of ICG and CTS in 4T1 cells and achieve excellent treatment effect, co-incubation of formulations with 4T1 cells for 4 h was selected as the best time for laser irradiation.

3.4. *In vitro* anticancer efficacy of (ICG + CTS)@HA-ZIF-8

The cytotoxicity of ICG, ICG(+L), CTS, ICG + CTS(+L), ICG@HA-ZIF-8(+L), CTS@HA-ZIF-8, (ICG + CTS)@ZIF-8(+L) and (ICG + CTS)@HA-ZIF-8 against 4T1 cells was examined with CCK-8 method. The cell viability of 4T1 cells after treatment with different formulations was shown in Fig. 2E and F. Compared to the group without laser irradiation, the cytotoxicity of 4T1 cells treated with the same formulation containing ICG was significantly enhanced after laser irradiation (cytotoxicity:ICG < ICG(+L); (ICG + CTS)@HA-ZIF-8< (ICG + CTS)@HA-ZIF-8 (+L)), indicating that ICG-containing formulations had a good anti-tumor effect on 4T1 tumor cells under laser irradiation conditions. Both single ICG and single CTS were less effective in inhibiting tumor cells compared to combination therapy (cytotoxicity: CTS < ICG(+L) < ICG + CTS(+L); CTS@HA-ZIF-8<ICG@HA-ZIF-8(+L)< (ICG + CTS) @HA-ZIF-8(+L)), suggesting a good synergistic effect of ICG and CTS. Compared to ICG + CTS(+L) and (ICG + CTS)@ZIF-8(+L), (ICG + CTS) @HA-ZIF-8(+L) exhibited the highest cytotoxicity against 4T1 cells, possibly due to the active targeting of HA-ZIF-8 nanoparticles, which

could more effectively deliver ICG and CTS into the cells, thereby showing better inhibition of tumor cell proliferation.

The *in vitro* cytotoxicity study had confirmed that (ICG + CTS)@HA-ZIF-8(+L) has a certain cytotoxic effect on 4T1 cells. Subsequent research was performed to determine the pro-apoptotic efficacy of the formulation on 4T1 cells. Apoptotic induction was assessed via Annexin V-FITC/PI dual staining, analyzed by flow cytometry. The results were shown in Fig. 2G and H. Compared to the control group and the groups without laser irradiation, 4T1 cells treated with the same formulation showed a significant increase in apoptosis levels after laser irradiation (apoptosis levels: (ICG + CTS)@HA-ZIF-8<(ICG + CTS)@HA-ZIF-8(+L), suggesting that ICG-containing formulations had a good effect on inducing apoptosis in 4T1 tumor cells with laser irradiation. Whether it was single ICG or single CTS, the level of induced apoptosis in 4T1 cells was weaker than that of combination therapy (apoptosis levels: CTS@HA-ZIF-8<ICG@HA-ZIF-8(+L)< (ICG + CTS)@HA-ZIF-8(+L), indicating that ICG and CTS had a good synergistic effect. Compared with ICG + CTS(+L) and (ICG + CTS)@ZIF-8(+L), (ICG + CTS)@HA-ZIF-8(+L) exhibited the highest cell apoptosis rate (83.11 %), possibly because HA-ZIF-8 had better active targeting compared to free drugs and ZIF-8, allowing for more effective drug delivery into the cells and thus showing a better inhibitory effect on inducing tumor cell apoptosis. These findings mirrored trends noted in cytotoxicity assay outcomes. The effects of the formulations on 4T1 cell migration were explored *in vitro* using a wound healing experiment. As delineated in Fig. 3A and B, the group treated with (ICG + CTS)@HA-ZIF-8(+L) exhibited a wound healing rate of a mere 14.36 %, which was significantly reduced in comparison with that of the ICG + CTS(+L), ICG@HA-ZIF-8(+L), CTS@HA-ZIF-8, (ICG + CTS)@ZIF-8(+L), and (ICG + CTS)@HA-ZIF-8 groups, indicating that the combination of ICG and CTS could significantly curtail the migration of 4T1 cells, and this inhibitory effect could be enhanced by HA-ZIF-8.

CTS could reduce the synthesis of ATP by interfering with glycolysis [13,22]. The quantitative glucose uptake assay in 4T1 cells treated with ICG(+L), ICG + CTS(+L), ICG@ZIF-8(+L),(ICG + CTS)@ZIF-8(+L), ICG@HA-ZIF-8(+L) and (ICG + CTS)@HA-ZIF-8(+L) (concentration of CTS = 7 μM) was performed to estimate the exact inhibition efficacy of CTS. As indicated in Fig. 3C, compared to ICG(+L), the glucose uptake in 4T1 cells significantly decreased after treatment with ICG + CTS(+L). Similarly, compared to ICG@ZIF-8(+L) or ICG@HA-ZIF-8(+L), the glucose uptake in 4T1 cells significantly decreased after treatment with (ICG + CTS)@ZIF-8(+L) or (ICG + CTS)@HA-ZIF-8(+L), indicating that CTS had the ability to reduced intracellular glucose uptake, whether in a free state or in (ICG + CTS)@ZIF-8 or (ICG + CTS)@HA-ZIF-8 formulation. A severe reduction in intracellular glucose uptake in tumour cells hinders glucose metabolism, leading to a reduction in ATP (one of the major metabolites of glycolysis) production. As shown in Fig. 3D, after CTS treatment, the level of cellular ATP in 4T1 cells was significantly decreased.

3.5. In vitro detection of PKM2 and HSPs by western blot

As mentioned above, CTS can inhibit the production of ATP by interfering with cellular glycolysis, while HSPs are ATP-reliant chaperone proteins whose biosynthesis, expression, and function depend on the level of ATP production. In the process of glucose metabolism, PKM2 in tumor cells can transfer the high-energy phosphate bond of phosphoenolpyruvate to adenosine diphosphate, thus generating ATP [15]. Therefore, reducing the expression of PKM2 can inhibit glycolysis and weaken the energy metabolism of breast cancer cells, cut off the energy supply of HSPs, and thus inhibit the production of HSPs, and weaken the heat resistance of tumor cells to PTT [13,22]. First, an evaluation of PKM2 expression in 4T1 cells treated with various formulations by WB experiment. As presented in Fig. 3E and F, PKM2 levels were highest in 4T1 cells post-treatment with ICG@HA-ZIF-8(+L), indicating that thermal stimulation caused by PTT could induce stress response in tumor cells, leading to increased expression of PKM2. The expressions of PKM2 in ICG + CTS(+L), (ICG + CTS)@ZIF-8(+L) and (ICG + CTS)@HA-ZIF-8(+L) groups were significantly lower compared to the ICG@HA-ZIF-8(+L) group, and the expression of PKM2 in (ICG + CTS)@HA-ZIF-8(+L) group was the lowest. These results indicated that the combination of ICG + CTS could reduce the expression of PKM2 in 4T1 cells, and this effect could be potentiated by HA-ZIF-8. Next, to investigate whether inhibiting glycolysis would interfere with the level of intracellular HSPs, this study detected the expression of HSP70 and HSP90 proteins in 4T1 cells treated with ICG + CTS(+L), ICG@HA-ZIF-8(+L), (ICG + CTS)@ZIF-8(+L), (ICG + CTS)@HA-ZIF-8(+L) (concentration of ICG = 4 μM) by WB. As shown in Fig. 3E and G, after treatment with ICG@HA-ZIF-8(+L), the expressions of HSP70 and HSP90 in 4T1 cells were the highest, indicating that the increase in temperature indeed stimulated tumor cells to produce heat protection and promote the expression of HSP70 and HSP90 proteins. The expressions of PKM2 in ICG + CTS(+L), (ICG + CTS)@ZIF-8(+L), and (ICG + CTS)@HA-ZIF-8(+L) were significantly lower compared to the ICG@HA-ZIF-8(+L) group, and the expression of HSP70 and HSP90 proteins in (ICG + CTS)@HA-ZIF-8(+L) group was the lowest. These results indicated that inhibiting glycolysis could effectively reduce the expressions of intracellular HSPs, and this effect could be enhanced by HA-ZIF-8. Therefore, (ICG + CTS)@HA-ZIF-8(+L) has great potential in significantly inhibiting the expression of HSPs by inhibiting glycolysis and reducing the production of ATP, thus improving the efficacy of PTT.

3.6. In vivo tumor targeting and NIR-II fluorescence imaging

Before *in vivo* studies, we first investigated the hemolytic potential of the formulations. As illustrated in Fig. 4A, the hemolysis rates of all formulations were less than 5 % at the actual *in vivo* dose, meeting the requirements for intravenous injection. All formulation groups demonstrated good blood safety when administered *in vivo*. Beyond its application in PTT, ICG could also be used as a fluorescent probe molecule enabling real-time observation of drug distribution within the body. Mice bearing orthotopic 4T1 tumors was established, and the *in vivo* distribution of the formulation was observed after intravenous injection. The appropriate time point for laser irradiation of the tumor site after intravenous injection was determined. As shown in Fig. 4B and E, 1 h after injection, the fluorescence signals of ICG, ICG@ZIF-8, and ICG@HA-ZIF-8 were the strongest at the tumor site, and this time point was chosen as time window for PTT in subsequent *in vivo* experiments. From then to until 24 h, the fluorescence signals of ICG@ZIF-8 and ICG@HA-ZIF-8 remained at a relatively high level, while the fluorescence signal of the ICG group barely disappeared. This might be related to the rapid excretion of ICG in the body and nanoparticles could ameliorate this phenomenon.Notably, the fluorescent signal from the ICG@HA-ZIF-8 formulation was consistently more pronounced when compared to ICG@ZIF-8, potentially due to the CD44-mediated active targeting mechanism. After 24 h, the mice were euthanized and dissected. The distribution of the formulations in the main organs and tumors was observed. As depicted in Fig. 4C and F, negligible fluorescence was detected in the organs and tumor sites in the ICG group, indicating that ICG had been metabolized. For the ICG@ZIF-8 and ICG@HA-ZIF-8 groups, strong fluorescence signals were observed in the livers, mainly because reticuloendothelial system (RES) was present in the livers, which could selectively uptake nanoparticles such as ICG@ZIF-8 and ICG@HA-ZIF- [23]. In addition, strong fluorescence signals were also detected at the tumor sites in the ICG@ZIF-8 and ICG@HA-ZIF-8 groups, which was also related to the EPR effect mediated by the nanoparticles, and the fluorescence signals of the ICG@HA-ZIF-8 group were stronger than that of the ICG@ZIF-8 group, which might be due to the active targeting effect mediated by CD44. The above results collectively indicated that ICG@HA-ZIF-8 had a strong tumor targeting ability, could accumulate in tumor tissues and provide necessary prerequisites for better exerting the therapeutic effect.

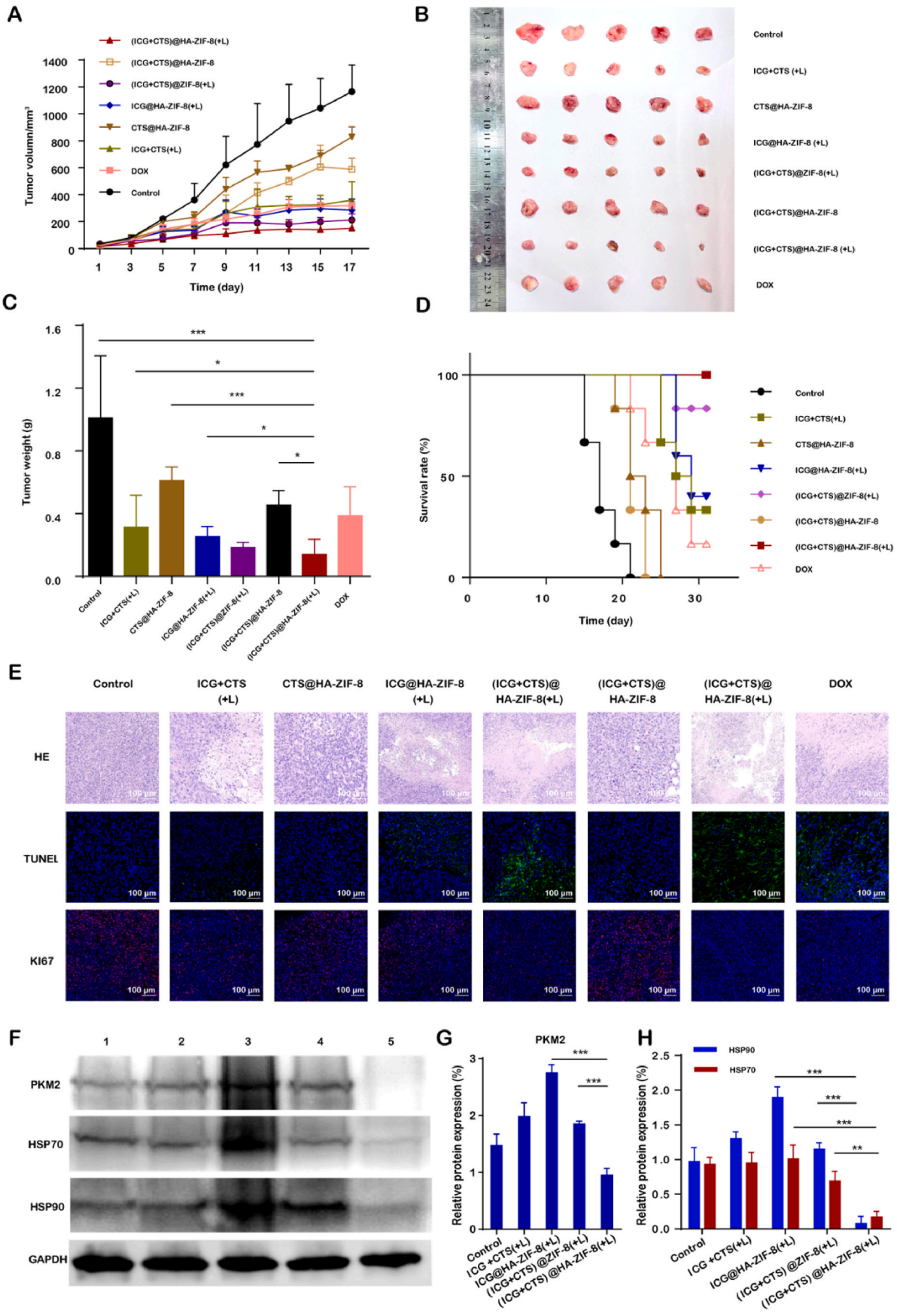

(caption on next page)

Fig. 5. The *in vivo* anticancer efficacy of formulations in mice bearing orthotopic 4T1 tumors: A) The tumor volume growth curves of mice bearing orthotopic 4T1 tumors after different treatments during 17 days. B) The photograph of the excised tumors after the last administration. C) The tumor weights of the excised tumors in different groups. D) Survival rate of mice within the observation period of 30 days in different treatment groups. E) HE, TUNEL and Ki67 staining of tumor sections excised from mice with different treatments. F) WB detection of PKM2 and HSP70/90 expressions in tumor sections excised from mice with different treatments (1: Control; 2:ICG + CTS(+L); 3:ICG@HA-ZIF-8(+L); 4:(ICG + CTS)@ZIF-8(+L); 5:(ICG + CTS)@HA-ZIF-8(+L). G) The statistical semi-quantification of detecting PKM2 expression in tumor sections excised from mice with different treatments. H) The statistical semi-quantification of detecting HSP70/90 expressions in tumor sections excised from mice with different treatments. (*: $P < 0.05$, **: $P < 0.01$, ***: $P < 0.001$, n = 5).

In order to study whether the formulation could achieve effective PTT under laser irradiation, we used infrared thermography to monitor the thermal response in mice 1 h after administration of saline (Control), ICG, ICG@ZIF-8, and ICG@HA-ZIF-8 under laser irradiation (1 W/cm^2, 808 nm). The results were shown in Fig. 4D and G, after 5 min of laser irradiation, tumor temperature remained relatively unchanged in the saline group. The tumor temperature in the ICG group increased by about 7.95 °C after laser irradiation, indicating a certain PTT effect. The temperature increase in the ICG@ZIF-8 and ICG@HA-ZIF-8 groups reached 9.85 °C and 10.95 °C respectively, achieving a good PTT effect. This result also indirectly confirmed the effective accumulation of ICG@ZIF-8 and ICG@HA-ZIF-8 at the tumor site, aligning with the *in vivo* distribution findings. The temperature increase of ICG@HA-ZIF-8 was stronger than that of ICG@ZIF-8, which might be due to the enhanced tumor-specific accumulation mediated by CD44, resulting in a higher drug concentration and a better therapeutic effect at the tumor site. These results demonstrated that ICG@HA-ZIF-8 could achieve good *in vivo* temperature rise effect under 808 nm laser irradiation.

3.7. In vivo anticancer efficacy of (ICG + CTS)@HA-ZIF-8

In vivo anti-tumor growth and metastasis pharmacological studies were conducted on mice bearing orthotopic 4T1 tumors. Fig. 5A,B,C & Fig. S6 showed the tumor growth curves and tumor images of each group after treatment. It could be observed that the tumor growth in saline group (Control) was rapid, while ICG@HA-ZIF-8(+L), CTS@HA-ZIF-8 and (ICG + CTS)@HA-ZIF-8 could exert a degree of tumor growth suppression. Compared with the free ICG + CTS(+L) group (tumor inhibition rate 69.22 %), the (ICG + CTS)@ZIF-8(+L) group (tumor inhibition rate 81.81 %) and (ICG + CTS)@HA-ZIF-8(+L) group (tumor inhibition rate 87.01 %) had stronger tumor growth inhibition, possibly owing to the improved retention and accumulation of the drug within the tumor facilitated by the nanoparticle carriers. Furthermore, the tumor suppression efficacy of (ICG + CTS)@HA-ZIF-8(+L) was significantly stronger than that of (ICG + CTS)@ZIF-8(+L) ($P < 0.05$), which might be due to the active targeting effect of HA-ZIF-8 mediated by CD44 in mice, leading to higher drug concentrations at the tumor sites and achieving a stronger synergistic effect, significantly enhancing the anti-tumor efficacy, which was stronger than the positive drug DOX. Consistent with the above results, mice treated with (ICG + CTS)@HA-ZIF-8(+L) had a survival rate of 100 % within 30 days, significantly higher than other groups (Fig. 5D).

Tumor tissues were collected on the 17th day of treatment for HE, Ki67, and TUNEL staining analysis to further substantiate the synergistic anti-tumor effect of (ICG + CTS)@HA-ZIF-8(+L). As shown in Fig. 5E, HE staining results showed significant apoptosis and necrosis in the tumor tissue of the (ICG + CTS)@HA-ZIF-8(+L) group, with typical features such as cell shrinkage and deepening of nuclear staining. TUNEL and Ki67 staining analysis further supported that the (ICG + CTS)@HA-ZIF-8(+L) group had the highest rate of cell apoptosis and the greatest inhibitory effect on tumor cell proliferation. Therefore, (ICG + CTS)@HA-ZIF-8(+L) achieved efficient anti-tumor effects by integrating tumor active targeting and synergistic action of ICG and CTS.

Concurrently, tumor tissues were taken for WB analysis and immunofluorescence staining to investigate the expression of PKM2 and HSPs to shed light on the molecular mechanism of the observed synergism in therapy. Fig. 5F,G,H&6A delineated that compared with saline group (Control), the expressions of PKM2, HSP70, and HSP90 in the ICG@HA-ZIF-8(+L) group were significantly increased, indicating that PTT could increase the expression of PKM2 and HSPs in tumor tissues. Compared with the ICG@HA-ZIF-8(+L), ICG + CTS(+L), and (ICG + CTS)@ZIF-8 (+L) groups, the expressions of PKM2, HSP70 and HSP90 in the (ICG + CTS)@HA-ZIF-8(+L) group were significantly decreased, indicating that the tumor-targeting property of HA-coated nanoparticles and the synergistic effect of ICG and CTS could reduce the expressions of PKM2 and HSPs in tumor tissues. The above results were consistent with the *in vitro* experimental results, which might be due to the increase of ICG and CTS in tumor cells, which reduced the expression of PKM2, interfered with the glycolysis of tumor cells, rapidly decreased ATP content, and further limited the expression of HSPs, weakened the heat protection effect in tumor cells, thereby potentiating the efficacy of PTT.

Reshaping the energy metabolism of breast cancer cells can curb both their proliferation and metastatic potential [10–12]. Therefore, we also evaluated the effect of (ICG + CTS)@ZIF-8(+L) on breast cancer lung metastasis in mice. On the 17th day of treatment, lung tissues from each group were collected, and picric acid staining was performed to observe the lung nodules of each group. Fig. 6 B&C revealed that in comparison to the saline group (Control), the number of lung nodules in each treatment group was reduced to some extent. ICG@HA-ZIF-8(+L), CTS@HA-ZIF-8 and (ICG + CTS)@HA-ZIF-8 could inhibit tumor metastasis to a certain extent. Compared with the free ICG + CTS(+L) group, DOX, (ICG + CTS)@ZIF-8(+L), and (ICG + CTS)@HA-ZIF-8 group had stronger inhibitory effects on tumor metastasis, among which (ICG + CTS)@HA-ZIF-8(+L) group had almost no lung nodules with the strongest inhibitory effect on breast cancer lung metastasis. The HE staining of lung tissues (Fig. 6D) corroborated the findings above. These results indicated that (ICG + CTS)@HA-ZIF-8(+L) might reduce the metabolic level of tumor cells by targeting glycolysis, reduce ATP production, not only inhibit the growth of breast cancer, overcome the heat tolerance of tumor cells, but also inhibit breast cancer metastasis, enhance PTT efficacy. We alao preliminarily evaluated the biosafety of the formulation in mice. The body weight of mice in each group slowly increased, and HE staining of major organs (Figs. S7 and 8) showed no pathological changes with no significant organ damage, indicating that the toxicity of the formulations could be ignored.

4. Conclusions

In view of TNBC metastasis and the heat resistance faced by tumor PTT, we designed a HA coated ZIF-8 drug delivery system loading with ICG and CTS. (ICG + CTS)@HA-ZIF-8 showed an increase in particle size, a reversal of charge from positive to negative and a rough surface, which indicated the successful coating of HA. The drug delivery system had excellent photothermal properties, which could reach temperature sufficient for photothermal ablation of tumor cells. (ICG + CTS)@HA-ZIF-8 also showed pH-dependent drug release, enhancing the sustained release of ICG and CTS to prolong drug retention in systemic circulation. HA-coated ZIF-8 enhanced the targeting ability of ZIF-8 *in vitro* and *in vivo* through the EPR effect alongside CD44-mediated tumor active targeting, resulting in a higher drug concentration and a better therapeutic effect in tumor. (ICG + CTS)@HA-ZIF-8 could downregulate the expression of glycolysis-related protein PKM2, thereby inhibiting the glycolysis process, further suppressing tumor cell energy metabolism, downregulating the expression of HSPs, overcoming tumor cell heat resistance, and improving PTT effect. These modulations not only hindered the proliferation of breast cancer cells but also their potential to

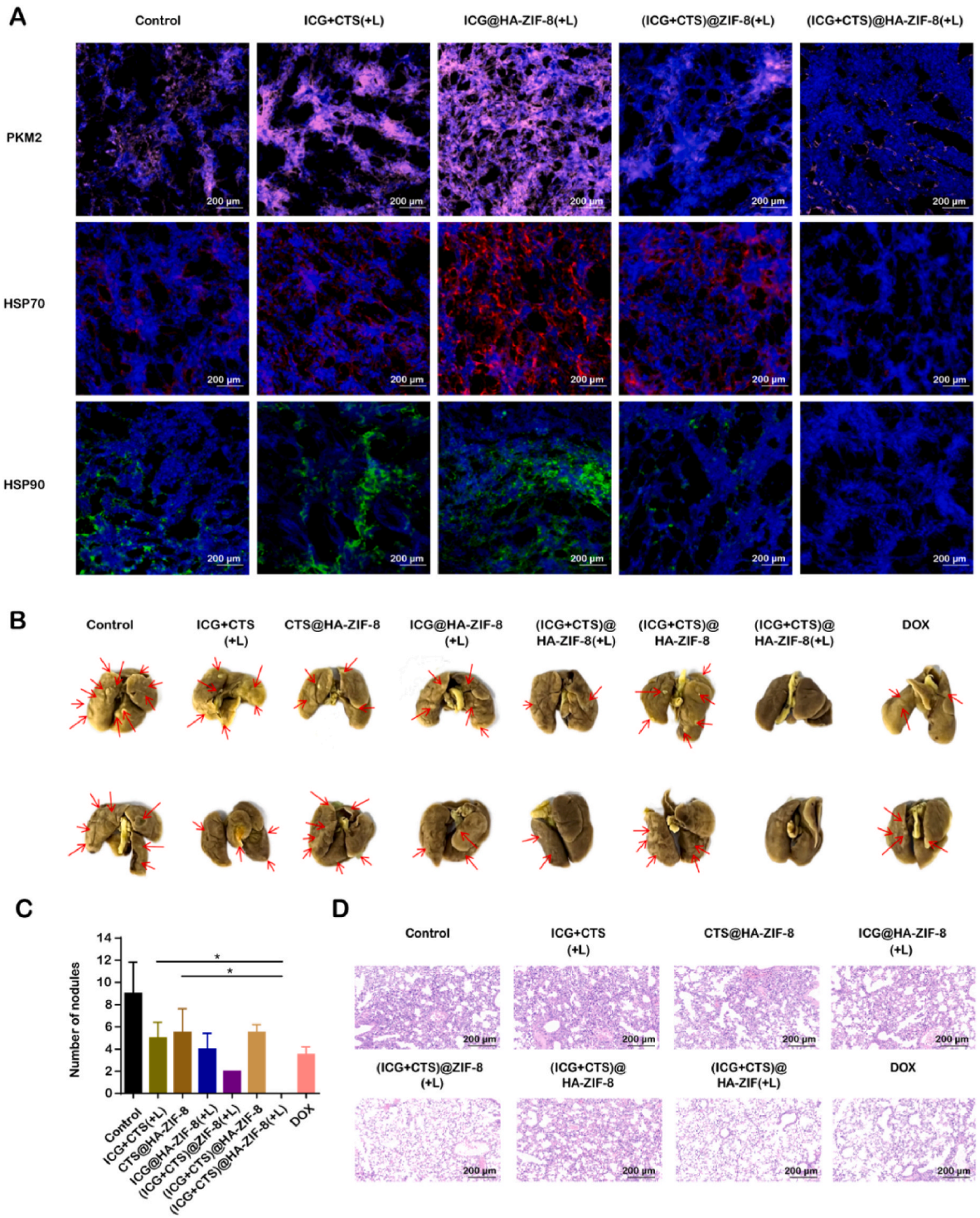

Fig. 6. The *in vivo* immunofluorescent staining of PKM2 and HSP70/90 and anti-metastasis effect of formulations in mice bearing orthotopic 4T1 tumors: A) Immunofluorescent staining of PKM2 (pink fluorescence), HSP70 (red fluorescence) and HSP90 (green fluorescence) in tumor sections excised from mice with different treatments. Cell nuclei were stained with DAPI (blue fluorescence). B) Images of lungs in different groups and the red arrows represented metastatic nodules on lungs. C) The quantitative analysis of node numbers. D) HE staining of lungs mice with different treatments. (*: $P < 0.05$,**: $P < 0.01$,***: $P < 0.001$,n = 5). (For interpretation of the references to colour in this figure legend, the reader is referred to the Web version of this article.)

metastasize, suggesting that this strategy could inspire innovative approaches for image-guided PTT in the management of breast cancer.

CRediT authorship contribution statement

Zhe Li: Writing – review & editing, Writing – original draft. **Liyan Sun:** Writing – review & editing, Writing – original draft. **Jinshuai Lan:** Supervision. **Ya Wu:** Writing – original draft, Data curation. **Siqi Yang:** Visualization, Data curation. **Tong Zhang:** Supervision. **Yue Ding:** Supervision.

Declaration of competing interest

The authors declare that they have no known competing financial interests or personal relationships that could have appeared to influence the work reported in this paper.

Data availability

Data will be made available on request.

Acknowledgements

This study was supported by "Shuguang Program" supported by Shanghai Education Development Foundation and Shanghai Municipal Education Commission (grant numbers 20SG43); Program of Shanghai Academic/Technology Research Leader (Grant 22XD1423000); Programs of the National Natural Science Foundation of China [grant number 82204777, 82374002 and 82274066]; Shanghai Science and technology innovation project (grant number 20S21902500 and 22S21901200); Program from the Shanghai Committee of Science and Technology (21010504200); Youth Talent Program from the Shanghai Municipal Health Commission (Grant 2022YQ030); Natural Science Foundation of Shanghai (grant number 21ZR1460800 and 22ZR1459000); National Key Research and Development Program of China (Grant 2022YFC3501705); China Postdoctoral Science Foundation [grant number 2022M712155].

Appendix B. Supplementary data

Supplementary data to this article can be found online at https://doi.org/10.1016/j.mtbio.2024.101200.

References

[1] H. Sung, J. Ferlay, R.L. Siegel, M. Laversanne, I. Soerjomataram, A. Jemal, F. Bray, Global cancer statistics 2020: GLOBOCAN estimates of incidence and mortality worldwide for 36 cancers in 185 Countries, CA Cancer J Clin 71 (2021) 209–249.
[2] R.L. Siegel, K.D. Miller, N.S. Wagle, A. Jemal, Cancer statistics, CA Cancer J Clin 73 (2023) 17–48, 2023.
[3] V. Thakur, R.V. Kutty, Recent advances in nanotheranostics for triple negative breast cancer treatment, J. Exp. Clin. Cancer Res. 38 (2019) 430.
[4] N. Harbeck, M. Gnant, Breast cancer, Lancet (N. Am. Ed.) 389 (2017) 1134–1150.
[5] L. Yin, J.J. Duan, X.W. Bian, S.C. Yu, Triple-negative breast cancer molecular subtyping and treatment progress, Breast Cancer Res. 22 (2020) 61.
[6] Y. Liu, X.Z. Zhu, Y. Xiao, S.Y. Wu, W.J. Zuo, Q. Yu, A.Y. Cao, J.J. Li, K.D. Yu, G. Y. Liu, J. Wu, T. Sun, J.W. Cui, Z. Lv, H.P. Li, X.Y. Zhu, Y.Z. Jiang, Z.H. Wang, Z. M. Shao, Subtyping-based platform guides precision medicine for heavily pretreated metastatic triple-negative breast cancer: the FUTURE phase II umbrella clinical trial, Cell Res. 33 (2023) 389–402.
[7] P. Xu, F. Liang, Nanomaterial-based tumor photothermal immunotherapy, Int. J. Nanomed. 15 (2020) 9159–9180.
[8] Q. Dong, X. Wang, X. Hu, L. Xiao, L. Zhang, L. Song, M. Xu, Y. Zou, L. Chen, Z. Chen, W. Tan, Simultaneous application of photothermal therapy and an anti-inflammatory prodrug using pyrene-aspirin-loaded gold nanorod graphitic nanocapsules, Angew Chem. Int. Ed. Engl. 57 (2018) 177–181.
[9] O. Warburg, On the origin of cancer cells, Science 123 (1956) 309–314.
[10] C.W. Tseng, W.H. Kuo, S.H. Chan, H.L. Chan, K.J. Chang, L.H. Wang, Transketolase regulates the metabolic switch to control breast cancer cell metastasis via the alpha-ketoglutarate signaling pathway, Cancer Res. 78 (2018) 2799–2812.
[11] S. Jiang, L.F. Zhang, H.W. Zhang, S. Hu, M.H. Lu, S. Liang, B. Li, Y. Li, D. Li, E. D. Wang, M.F. Liu, A novel miR-155/miR-143 cascade controls glycolysis by regulating hexokinase 2 in breast cancer cells, EMBO J. 31 (2012) 1985–1998.
[12] G. Deblois, V. Giguere, Oestrogen-related receptors in breast cancer: control of cellular metabolism and beyond, Nat. Rev. Cancer 13 (2013) 27–36.
[13] J. Dang, H. Ye, Y. Li, Q. Liang, X. Li, L. Yin, Multivalency-assisted membrane-penetrating siRNA delivery sensitizes photothermal ablation via inhibition of tumor glycolysis metabolism, Biomaterials 223 (2019) 119463.
[14] X. Yao, W. Li, L. Li, M. Li, Y. Zhao, D. Fang, X. Zeng, Z. Luo, YTHDF1 upregulation mediates hypoxia-dependent breast cancer growth and metastasis through regulating PKM2 to affect glycolysis, Cell Death Dis. 13 (2022) 258.
[15] J. Zhou, C.M. Su, H.A. Chen, S. Du, C.W. Li, H. Wu, S.H. Tsai, Y.T. Yeh, Cryptanshinone inhibits the glycolysis and inhibits cell migration through PKM2/beta-catenin Axis in breast cancer, OncoTargets Ther. 13 (2020) 8629–8639.
[16] T. Wang, S. Li, Z. Zou, L. Hai, X. Yang, X. Jia, A. Zhang, D. He, X. He, K. Wang, A zeolitic imidazolate framework-8-based indocyanine green theranostic agent for infrared fluorescence imaging and photothermal therapy, J. Mater. Chem. B 6 (2018) 3914–3921.
[17] S. Yu, S. Wang, Z. Xie, S. Yu, L. Li, H. Xiao, Y. Song, Hyaluronic acid coating on the surface of curcumin-loaded ZIF-8 nanoparticles for improved breast cancer therapy: an in vitro and in vivo study, Colloids Surf. B Biointerfaces 203 (2021) 111759.
[18] E. Obaid, S. Wu, Y. Zhong, M. Yan, L. Zhu, B. Li, Y. Wang, W. Wu, G. Wang, pH-Responsive hyaluronic acid-enveloped ZIF-8 nanoparticles for anti-atherosclerosis therapy, Biomater. Sci. 10 (2022) 4837–4847.
[19] G. Gao, X. Sun, G. Liang, Nanoagent-promoted mild-temperature photothermal therapy for cancer treatment, Adv. Funct. Mater. 31 (2021) 2100738.
[20] T. Park, S. Lee, R. Amatya, H. Cheong, C. Moon, H.D. Kwak, K.A. Min, M.C. Shin, ICG-loaded PEGylated BSA-silver nanoparticles for effective photothermal cancer therapy, Int. J. Nanomed. 15 (2020) 5459–5471.
[21] V.D. Nguyen, H.K. Min, C.S. Kim, J. Han, J.O. Park, E. Choi, Folate receptor-targeted liposomal nanocomplex for effective synergistic photothermal-chemotherapy of breast cancer in vivo, Colloids Surf. B Biointerfaces 173 (2019) 539–548.
[22] Y. Yang, Y. Cao, L. Chen, F. Liu, Z. Qi, X. Cheng, Z. Wang, Cryptotanshinone suppresses cell proliferation and glucose metabolism via STAT3/SIRT3 signaling pathway in ovarian cancer cells, Cancer Med. 7 (2018) 4610–4618.
[23] Y. Tang, X. Wang, J. Li, Y. Nie, G. Liao, Y. Yu, C. Li, Overcoming the reticuloendothelial system barrier to drug delivery with a "Don't-Eat-Us" strategy, ACS Nano 13 (2019) 13015–13026.